Surface-emitting circular DFB, disk-, and ring-Bragg resonator lasers with chirped gratings. III: gain saturation effects and above-threshold analysis

Xiankai Sun[*] and Amnon Yariv

Department of Applied Physics, MC 128-95, California Institute of Technology, Pasadena, CA 91125, USA
[*]Corresponding author: xksun@caltech.edu

Abstract: As Part III of this series, this paper focuses on an above-threshold modal analysis which includes gain saturation effects in the surface-emitting chirped circular grating lasers. We derive an exact energy relation which states that, in steady state, the net power generated in the gain medium is equal to the sum of peripheral leakage power and vertical emission power. This relation is particularly useful in checking the accuracy of numerical mode solving. Numerical simulations demonstrate the dependence of required pump level on the vertical emission power and compare the laser threshold and energy conversion efficiency under uniform, Gaussian, and annular pump profiles. A larger overlap between the pump profile and modal intensity distribution leads to a lower threshold and a higher energy conversion efficiency. Finally the dependence of required pump level on device sizes offers us new design guidelines of these lasers for single-mode, high-efficiency, high-power applications.

References and links

1. T. Erdogan and D. G. Hall, "Circularly symmetric distributed feedback semiconductor lasers: an analysis," J. Appl. Phys. **68**, 1435-1444 (1990).
2. C. Wu, M. Svilans, M. Fallahi, T. Makino, J. Glinski, C. Maritan, and C. Blaauw, "Optical pumped surface-emitting DFB GaInAsP/InP lasers with circular grating," Electron. Lett. **27**, 1819-1821 (1991).
3. A. Jebali, R. F. Mahrt, N. Moll, D. Erni, C. Bauer, G.-L. Bona, and W. Bachtold, "Lasing in organic circular grating structures," J. Appl. Phys. **96**, 3043-3049 (2004).
4. G. A. Turnbull, A. Carleton, A. Tahraouhi, T. F. Krauss, I. D. W. Samuel, G. F. Barlow, and K. A. Shore, "Effect of gain localization in circular-grating distributed feedback lasers," Appl. Phys. Lett. **87**, 201101 (2005).
5. Y. Chen, Z. Li, Z. Zhang, D. Psaltis, and A. Scherer, "Nanoimprinted circular grating distributed feedback dye laser," Appl. Phys. Lett. **91**, 051109 (2007).
6. J. Scheuer and A. Yariv, "Coupled-waves approach to the design and analysis of Bragg and photonic crystal annular resonators," IEEE J. Quantum Electron. **39**, 1555-1562 (2003).
7. X. K. Sun and A. Yariv, "Surface-emitting circular DFB, disk-, and ring- Bragg resonator lasers with chirped gratings: a unified theory and comparative study," Opt. Express **16**, 9155-9164 (2008).
8. X. K. Sun and A. Yariv, "Surface-emitting circular DFB, disk-, and ring- Bragg resonator lasers with chirped gratings. II: nonuniform pumping and far-field patterns," Opt. Express **17**, 1-6 (2009).
9. H. A. Haus, "Gain saturation in distributed feedback lasers," Appl. Opt. **14**, 2650-2652 (1975).
10. K. J. Kasunic and M. Fallahi, "Gain satuation in circular-grating distributed-feedback semiconductor lasers," J. Opt. Soc. Am. B **14**, 2147-2152 (1997).
11. A. M. Shams-Zadeh-Amiri, X. Li, and W. P. Huang, "Above-threshold analysis of second-order circular-grating DFB lasers," IEEE J. Quantum Electron. **36**, 259-267 (2000).
12. T. Kossek and P. Szczepanski, "Nonlinear operation of a planar circular-grating DBR laser," IEEE J. Quantum Electron. **37**, 742-751 (2001).

13. X. K. Sun and A. Yariv, "Modal properties and modal control in vertically emitting annular Bragg lasers," Opt. Express **15**, 17323-17333 (2007).

1. Introduction

Surface-emitting circular grating lasers are considered a promising next-generation on-chip light source for optical communications which may substitute the prevailing VCSELs due to their circularly-symmetric, large-emission-aperture, narrow-divergence laser emission. There have been intensive research activities since early 1990s. Erdogan and Hall were the first to analyze their modal behavior with a scalar coupled-mode theory [1]. Wu *et al.* were the first to experimentally realize such lasers in semiconductors [2]. More recently, organic polymers are also used as the gain medium for these lasers due to their low fabrication cost [3-5].

The circular gratings in most of the work are designed radially periodic. In 2003 we proposed using radially chirped gratings to achieve optimal interaction with the optical fields, since the eigenmodes of the wave equation in cylindrical coordinates are Hankel functions [6]. As the grating designs follow the phases of Hankel functions, such circular grating lasers usually take three configurations shown in Fig. 1(a) circular DFB laser, (b) disk Bragg resonator laser, and (c) ring Bragg resonator laser. Including a second-order Fourier component, the gratings are able to provide in-plane feedback as well as couple laser emission out of the resonator plane.
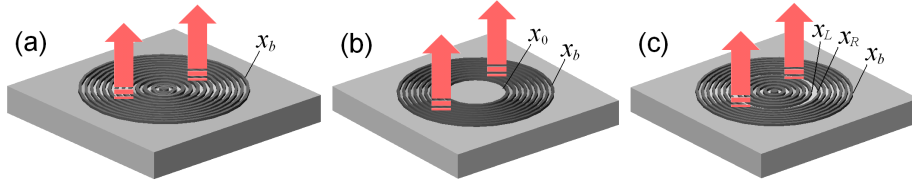
Fig. 1. Surface-emitting chirped circular grating lasers: (a) circular DFB laser; (b) disk Bragg resonator laser; (c) ring Bragg resonator laser. Laser emission is coupled out of the resonator plane in vertical direction via the gratings.

In previous parts of this paper series [7, 8], we have solved the modes and compared the modal properties, by both analytical and numerical approaches, of the three types of lasers at threshold. Gain saturation effects in above-threshold operation were previously studied in both linear and circular DFB and DBR lasers [4, 9-12]. This paper presents an above-threshold analysis for the three types of radially chirped circular grating lasers to investigate their energy conversion efficiency, intensity-dependent modal selectivity, and optimal design.

2. Energy relation

The basic equations that govern the modal behaviors in such Hankel-phased active circular grating structures have been derived in [13]:

$$\frac{dA(x)}{dx} = u(x) \cdot A(x) - v \cdot B(x) \cdot e^{2i\delta x}, \tag{1a}$$

$$\frac{dB(x)}{dx} = -u(x) \cdot B(x) + v \cdot A(x) \cdot e^{-2i\delta x}, \tag{1b}$$

where

$A(x)$ and $B(x)$: amplitudes of the in-plane outward and inward propagating cylindrical waves;

$x = \beta\rho$: normalized radial coordinate with β being the in-plane propagation constant;

$\delta = (\beta_{\text{design}} - \beta)/\beta$: frequency detuning factor, representing the relative frequency shift from the optimal coupling design;

$u(x) = g_A(x) - h_1$ and $v = h_1 + ih_2$;

$h_1 = h_{1r} + ih_{1i}$: radiation coupling coefficient, representing the effects of vertical emission;

h_2: feedback coupling coefficient (can always be chosen real);

$g_A(x) = g(x) - \alpha$: space-dependent net gain coefficient;

α: nonsaturable internal loss, including absorption and nonradiative scattering losses;

$g(x) = g_0(x)/[1 + I(x)/I_{sat}]$: intensity-dependent saturated gain profile;

$g_0(x)$: unsaturated gain profile; and

$I(x)/I_{sat}$: field intensity distribution in units of saturation intensity.

All the three types of circular grating lasers share the same boundary conditions [7]: (i) $A(0) = B(0)$; (ii) $B(x_b) = 0$; (iii) $A(x)$ and $B(x)$ continuous for $0 < x < x_b$. Once Eqs. (1a) and (1b) are solved with these boundary conditions, the in-plane electric field $E(x) = A(x)H_m^{(1)} + B(x)H_m^{(2)}$.

Assuming a linear pump–gain relationship above transparency, the unsaturated gain $g_0(x)$ follows the profile of pump intensity $I_{pump}(x)$, and we may define an experimentally measurable quantity: pump level $P_{pump} \equiv \int I_{pump}(x) \cdot 2\pi\rho \cdot d\rho = P_0 \int g_0(x) \cdot x \cdot dx$, where P_0 having a power unit is an experimental parameter determined by pumping scheme (electrical or optical) and specific setup configuration. For some simple g_0 profiles, P_{pump} has analytical expressions [8], otherwise, numerical integration always remains a resort.

Similar to the procedure in [9], multiplying Eq. (1a) by A^* and Eq. (1b) by B^*, then adding each equation to its complex conjugate, one obtains

$$\frac{d|A|^2}{dx} = 2\left(g_A - h_{1r}\right)|A|^2 - v \cdot A^*B \cdot e^{2i\delta x} - v^* \cdot AB^* \cdot e^{-2i\delta x}, \tag{2a}$$

$$\frac{d|B|^2}{dx} = -2\left(g_A - h_{1r}\right)|B|^2 + v \cdot AB^* \cdot e^{-2i\delta x} + v^* \cdot A^*B \cdot e^{2i\delta x}. \tag{2b}$$

Subtracting Eq. (2b) from Eq. (2a) yields

$$\frac{d}{dx}\left(|A|^2 - |B|^2\right) = 2g_A\left(|A|^2 + |B|^2\right) - 2h_{1r}\left|Ae^{-i\delta x} + Be^{i\delta x}\right|^2. \tag{3}$$

Integrating Eq. (3) from $x = 0$ to $x = x_b$ and applying $A(0) = B(0)$ and $B(x_b) = 0$ lead to

$$\underbrace{\left|A(x_b)\right|^2}_{\text{peripheral leakage}} + \underbrace{2h_{1r}\int_{\text{grating}}\left|Ae^{-i\delta x} + Be^{i\delta x}\right|^2 dx}_{\text{vertical laser emission}} = \underbrace{2\int_0^{x_b} g_A\left(|A|^2 + |B|^2\right)dx}_{\text{power generated in the gain medium}}, \tag{4}$$

which is the energy conservation theorem for the surface-emitting circular grating lasers. This equation is exact and states that, in steady state, the net power generated in the gain medium equals the sum of peripheral leakage power and vertical emission power. Due to its exactness, this relation is particularly useful in monitoring the accuracy of numerical mode solving.

It should be noted that the amplitudes A and B are dimensionless, and they can be scaled up or down arbitrarily. A judicious choice would be to normalize them such that the resulting intensity is normalized to the saturation intensity I_{sat}. Since $I(x) = cn\varepsilon_0|E|^2/2$ (c, the speed of light; n, transverse effective index; ε_0, the vacuum permittivity), if E_{sat} is similarly defined as $(2I_{sat}/cn\varepsilon_0)^{1/2}$, then the peripheral leakage power in real dimensions will be $\left|A(x_b)H_m^{(1)}(x_b)\right|^2 E_{sat}^2 \cdot 2\pi x_b D/\beta \approx \left|A(x_b)\right|^2 \cdot E_{sat}^2 \, 4D/\beta$, where D is the thickness of the laser resonator. A comparison of this expression with the first term on the left-hand side of Eq. (4) indicates that all the power terms are in units of the saturation power $P_{sat} \equiv E_{sat}^2 \, 4D/\beta$.

3. Numerical method

When solving the modes at threshold with uniform gain (or pump) distribution across the device, gain saturation effects can be ignored and Eqs. (1a) and (1b) have analytical solutions [7]. In case of using a nonuniform pump profile and/or taking into account the gain saturation effects in above-threshold operation, Eqs. (1a) and (1b) have to be numerically solved: starting with an amplitude set $[A \; B] = A(0)[1 \; 1]$ at the center, these equations are integrated

along x to the exterior boundary x_b. The absolute value of $B(x_b)$ marks a contour map in the two-dimensional plane of g_0 and δ. Each minimum point in the contour map represents a mode with corresponding g_0 and δ. Substituting the modal g_0, δ, $A(x)$, and $B(x)$ into Eq. (4), one immediately finds the mode-solving accuracy by comparing the left-hand and right-hand sides of the equation. The second term on the left-hand side of Eq. (4) is the surface emission power P_{em} in units of the saturation power P_{sat}. Inserting the modal g_0 into the expression for P_{pump} gives the required pump level.

During the numerical integration, an expression for the radial intensity distribution $I(x)$ is required. The expression for the electric field $E(x) = AH_m^{(1)} + BH_m^{(2)}$ leads straightforwardly to

$$I(x) = \left|E(x)\right|^2 = \left|AH_m^{(1)}\right|^2 + \left|BH_m^{(2)}\right|^2 + \underbrace{A^*BH_m^{(1)*}H_m^{(2)} + AB^*H_m^{(1)}H_m^{(2)*}}_{\text{interference terms}}. \tag{5}$$

In a gain medium, the motional nature of the electrons prevents them from sensing the fast-oscillating interference terms in Eq. (5). Therefore, with large-radius approximations of $H_m^{(1)}$ and $H_m^{(2)}$, Kasunic *et al.* dropped these interference terms and simplified the expression [10]. However, the remaining first two terms blow up at $x = 0$, which results in a dubious representation of $I(x)$ near the center. Here we suggest approximating $I(x)$ piecewise:

$$I(x) = \begin{cases} \left|AH_m^{(1)} + BH_m^{(2)}\right|^2, & x \leq x_{eq} \\ 2\left(|A|^2 + |B|^2\right)\big/\pi x, & x > x_{eq}. \end{cases}$$

The criterions for choosing the joint point x_{eq} are: first, to ensure the continuity of $I(x)$, x_{eq} has to be where the interference terms vanish, i.e., at a zero of the interference terms; second, x_{eq} has to precede the start of the fast oscillation of $I(x)$; third, the choice of x_{eq} has to validate the approximation for $I(x)$ at $x > x_{eq}$. Based on the modal profiles, x_{eq} is chosen to be the second zero of the interference terms, which is 1.76.

4. Numerical results and discussions

The laser structural parameters are assumed to be the same as those in [7] and [8]. In short, in grating regions $h_1 = 0.0072 + 0.0108i$ and $h_2 = 0.0601$ while in no-grating regions both vanish. For comparison purposes, all the three types of lasers share an x_b. In addition, for disk Bragg resonator laser $x_0 = x_b/2$, and for ring Bragg resonator laser $x_L = x_b/2 - \pi$ and $x_R = x_b/2 + \pi$. The only parameter related to material is the nonsaturable internal loss α, which is assumed to be 0.2×10^{-3} (normalized by β) for typical III–V quantum well lasers.

4.1. Gain saturation effects on the laser modes
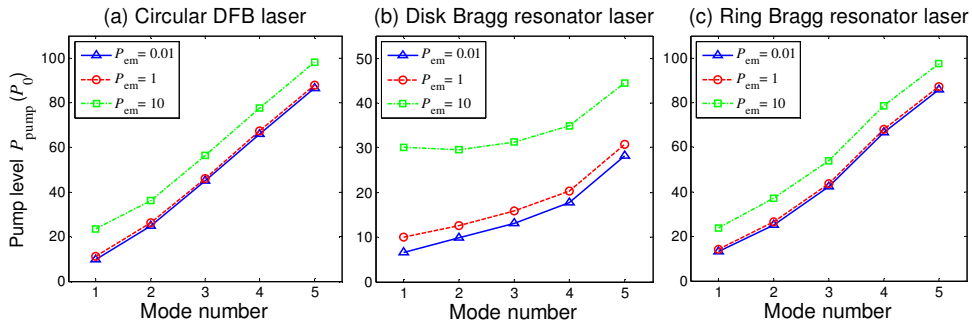
Fig. 2. Pump level P_{pump} of the 5 lowest order modes, under uniform pump profile, of (a) circular DFB, (b) disk-, and (c) ring- Bragg resonator lasers with surface emission power $P_{em} = 0.01$, 1, and 10 (in units of saturation power P_{sat}).

To demonstrate the gain saturation effects on the laser modes, a typical device size $\rho_b = 17.5$ μm ($x_b = \beta\rho_b \approx 200$) is assumed for all the circular DFB, disk-, and ring- Bragg resonator lasers. Figure 2 displays pump level P_{pump} of the 5 lowest order modes, under uniform pump profile, of these three types of lasers with surface emission power $P_{\text{em}} = 0.01$, 1, and 10 (in units of saturation power P_{sat}). The features are summarized as follows: (i) At low surface emission $P_{\text{em}} = 0.01$ and 1, disk Bragg resonator laser always possesses the lowest P_{pump} out of the three types, while at high surface emission $P_{\text{em}} = 10$, P_{pump} of Mode 1 of disk Bragg resonator laser is greatly enhanced and even higher than that of circular DFB and ring Bragg resonator lasers. (ii) Disk Bragg resonator laser has smaller discrimination between the modes compared with that of circular DFB and ring Bragg resonator lasers, and as a result the difference in gain saturation levels can easily change the order of the modes: Mode 2 exhibits even lower P_{pump} than Mode 1 at $P_{\text{em}} = 10$. This mode transition behavior will be illustrated more clearly in the device-size-dependent P_{pump} curves shown in Fig. 3.

4.2. Above-threshold behavior: comparison of threshold pump level and energy conversion efficiency with different pump profiles

By varying the boundary condition $A(0)$ in the integration process, we are able to get the (P_{pump}, P_{em}) pairs which basically form the typical input–output relation for a laser mode. The laser threshold P_{th} is the pump level at the onset of surface laser emission. The energy conversion efficiency (or external differential efficiency) η_{ex} is defined as the slope $dP_{\text{em}}/dP_{\text{pump}}$ of the linear fit of the simulated data points up to $P_{\text{em}} = 10$. To compare the effects of different pump profiles, P_{th} and η_{ex} of Mode 1 of the three types of lasers were calculated under uniform, Gaussian, and annular pump profiles. The Gaussian profile is assumed to follow $g_0(x) = g_0 \exp\left[-x^2/w_p^2\right]$ with $w_p = x_b/2 = 100$. The annular profile is assumed to follow $g_0(x) = g_0 \exp\left[-(x-x_p)^2/w_p^2\right] + g_0 \exp\left[-(x+x_p)^2/w_p^2\right]$ with $x_p = x_b/2 = 100$ and $w_p = x_b/4 = 50$. The results are listed in Table 1.

Table 1. Threshold pump level P_{th} (in units of P_0) and energy conversion efficiency η_{ex} (in units of P_{sat}/P_0) of circular DFB, disk-, and ring- Bragg resonator lasers under different pump profiles

Pump profile	Circular DFB laser		Disk Bragg resonator laser		Ring Bragg resonator laser	
	P_{th}	η_{ex}	P_{th}	η_{ex}	P_{th}	η_{ex}
Uniform	9.760	0.7369	6.565	0.4374	13.162	0.9278
Gaussian	5.967	0.9961	2.373	0.8741	8.570	1.379
Annular	6.382	0.9742	5.855	0.7358	7.010	1.500

Clearly a low P_{th} and a high η_{ex} always come together. The lowest P_{th} and the highest η_{ex} are achieved with the Gaussian pump for circular DFB and disk Bragg resonator lasers and with the annular pump for ring Bragg resonator laser. Actually P_{th} and η_{ex} are both related to the overlap between pump profile and modal intensity distribution [8]. A larger overlap results in more efficient energy conversion in the gain medium which consequently leads to a lower P_{th} and a higher η_{ex}.

4.3. Revisit of modal selectivity and optimal design

Figure 3 shows device-size-dependent pump level P_{pump} and frequency detuning factor δ of the 3 lowest order modes, under uniform pump profile, of the three types of lasers. The modes are numbered in accord with those in Fig. 2. For both P_{pump} and δ, dashed lines mark their values obtained at threshold and solid lines at $P_{\text{em}} = 10$.

Examined from the plots, at high emission level $P_{\text{em}} = 10$, circular DFB and ring Bragg resonator lasers still possess large discrimination between the modes, which ensures them a large single-mode range of at least 50–250. Additionally, we identify low-pump ranges for their Mode 1 at $P_{\text{em}} = 10$, which are 100–160 for circular DFB laser and 80–130 for ring

Bragg resonator laser. The existence of a low-pump range is a result of competition between the pumped area and the required gain level: although larger devices require a larger area to be pumped, their longer radial Bragg gratings reduce the needed gain because of stronger reflection of the optical fields from the gratings. The low-pump range is an important factor in designing high-efficiency, high-power lasers.

The P_{pump} for disk Bragg resonator laser exhibits interesting behaviors: (i) at $x_b = 200$, the order of Modes 1 and 2 exchanges from at threshold to at high surface emission level due to the participation of gain saturation effects; (ii) the single-mode range (for Mode 2) shifts from 60–140 at threshold to 90–175 at $P_{\text{em}} = 10$. Therefore the single-mode range for engineering should be the overlap of these two sets, which is 90–140.

On the other hand, all the frequency detuning factors δ are almost unaffected by the surface emission level (as seen from the overlap of dashed and solid lines in the lower plots), since δ is an intrinsic property of a laser mode.
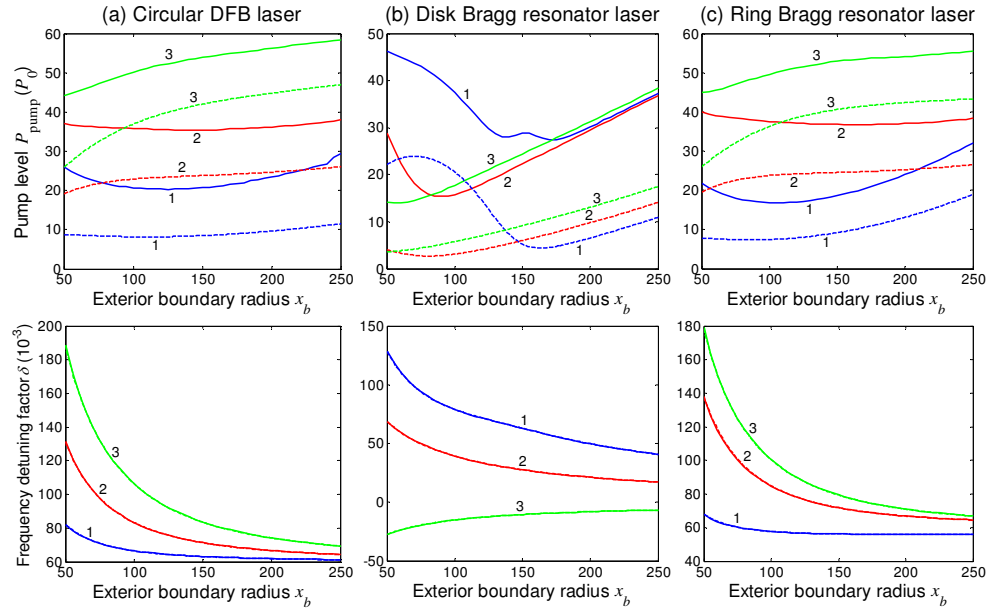
Fig. 3. Device-size-dependent pump level P_{pump} and frequency detuning factor δ of the 3 lowest order modes, under uniform pump profile, of (a) circular DFB, (b) disk-, and (c) ring- Bragg resonator lasers. x_b is the exterior boundary radius for all types of lasers. The inner disk radius x_0 of disk Bragg resonator laser is set to be $x_b/2$. The inner and outer edges of the annular defect of ring Bragg resonator laser are set to be $x_L = x_b/2 - \pi$ and $x_R = x_b/2 + \pi$. The modes are labeled in accord with those shown in Fig. 2. Dashed lines mark the values obtained at threshold and solid lines at $P_{\text{em}} = 10$.

5. Conclusions

An above-threshold analysis, including gain saturation effects, on the modal properties of surface-emitting chirped-grating circular DFB, disk-, and ring- Bragg resonator lasers has been performed. An exact energy relation in such surface-emitting lasers was derived, which is interpreted as the energy conservation theorem: in steady state, the net power generated in the gain medium is equal to the sum of peripheral leakage power and vertical emission power.

Numerical simulations demonstrated the dependence of required pump level on the vertical emission power for each laser mode. The threshold pump level P_{th} and energy conversion efficiency η_{ex} were compared under three pump profiles − uniform, Gaussian, and annular. A larger overlap between the pump profile and modal intensity distribution leads to a lower P_{th} and a higher η_{ex}.

Finally, as shown in the evolution of modal pump levels with the device size, disk Bragg resonator laser exhibits mode transition behavior which modifies its single-mode range, while circular DFB and ring Bragg resonator lasers find each low-pump range. These numerical results provide us useful information in designing such lasers for single-mode, high-efficiency, high-power applications.

Acknowledgments